From continuum analytical description to discrete numerical modelling of localized fluidization in granular media

Eduard Puig i Montellà[1,⋆], *Marcella* Toraldo[1], *Bruno* Chareyre[1,⋆⋆], and *Luc* Sibille[1,⋆⋆⋆]

[1] *Grenoble Institut of Technology (G-INP), University Grenoble Alpes (UGA), 3SR, F-38000 Grenoble, France.*

Abstract. We present analytical and numerical results on localized fluidization within a granular layer subjected to a local injection of fluid. As the injection rate increases the three different regimes previously reported in the literature are recovered: homogeneous expansion of the bed, fluidized cavity in which fluidization starts developing above the injection area, and finally the chimney of fluidized grains when the fluidization zone reaches the free surface. The analytical approach is at the continuum scale, based on Darcy's law and Therzaghi's effective stress principle. It provides a good description of the phenomenon as long as the porosity of the granular assembly remains relatively homogeneous. The numerical approach is at the particle scale based on the coupled DEM-PFV method. It tackles the more heterogeneous situations which occur at larger injection rates. A direct link is evidenced between the occurrence of the different regimes of fluidization and the injection aperture. Finally, the merging of chimneys in case of two injection points is investigated.

1 Introduction

Fluidization refers to the fluid-solids systems in which the solid phase in a granular material is subjected to behave like a fluid by an upward seepage flow [1]. Fluidization is employed in a wide variety of industrial processes such as heat transfer, petroleum refining, coal conversion and water treatment [2, 3].

A specific case concerns very localized influx of fluid, inducing a spatial heterogeneity of the phenomenon inside the grains packing, this situation is known as localized fluidization.

A typical configuration for laboratory experiments on localized fluidization is shown in figure 1. The granular layer is initially at static equilibrium then subjected to one or several local injections of fluid through the bottom face of the box (figure 1). The previous works on such configurations evidenced three successive regimes during a gradual increase of the injection rate [4–7]. At very low rates, the bed is stable. Larger rates cause bed expansion even before any fluidization zone can be observed (expansion regime). For a yet larger rate, the hydrodynamic forces exerted on some particles are sufficient to counterbalance their weight, triggering movements above the injection point in the so called "fluidized" zone (cavity regime). Eventually, the height of the fluidized zone increases with the injection rate, until it reaches the top of the granular layer (chimney regime). Numerical simulations were found to match qualitatively with available experimental data [8].

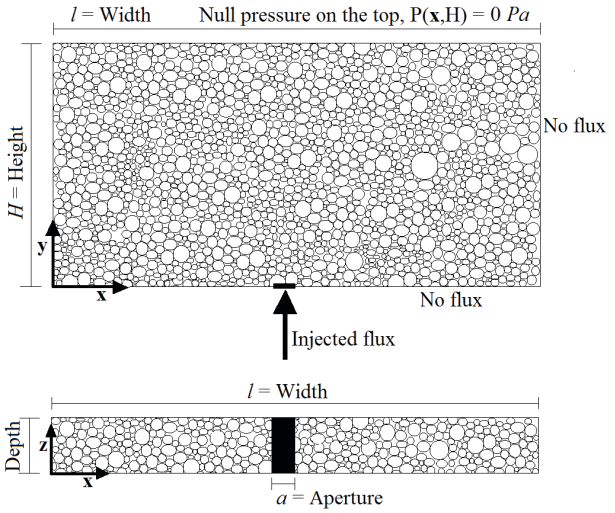

Figure 1. Sample geometry and boundary conditions.

Crude simplifications are required to find an analytical solution due to the nonlinear process. Nevertheless, it will be seen that a continuum scale model can give some insight into some governing mechanisms as the analytical model predicts the transitions between the different regimes and it provides a simple framework to explain the main trends. In this work, we provide closed form solutions for the field of initial pore pressure in the problem of figure 1.

In order to overcome this drawback and obtain a more realistic simulation of the process, a numerical model of grain-fluid systems is proposed. In this work we use a

⋆ e-mail: eduard.puigmontella@3sr-grenoble.fr
⋆⋆ e-mail: bruno.chareyre@3sr-grenoble.fr
⋆⋆⋆ e-mail: luc.sibille@ujf-grenoble.fr

Table 1. Physical and geometrical variables of the problem. The dimensions are defined in the [FLT] (force, length, time) system.

Variable	Dimension	SI units
Discharge per unit depth (q)	$L^2 \cdot T^{-1}$	$[m^2/s]$
Pressure (P)	FL^{-2}	$[Pa]$
Height (H)	L	$[m]$
Length (l)	L	$[m]$
Grain diameter (D)	L	$[m]$
Dynamic viscosity (μ)	$FL^{-2}T$	$[Pa \cdot s]$
Aperture(a)	L	$[m]$
Weight density, solid (γ_s)	FL^{-3}	$[N \cdot m^{-3}]$
Weight density, fluid (γ_w)	FL^{-3}	$[N \cdot m^{-3}]$
Porosity (n)	–	$[-]$

coupling between the discrete element method and a pore-scale finite volume method (DEM-PFV) [9, 10] to simulate the complete process from the expansion regime to the chimney regime.

2 Methodology

2.1 Problem statement

As a model system, we consider a layer of quasi monodisperse spheres immersed in a viscous fluid inside a rigid box. The system is subjected to gravity and the density of the solid particles is larger than that of the fluid. The physical variables of the problem are summarized in table 1.

2.2 Dimensionless variables

Based on the above variables we introduce the so-called submerged density $\gamma' = (1-n)(\gamma_s - \gamma_w)$, and the reference vertical effective stress:

$$\sigma'_0 = (1-n)(\gamma_s - \gamma_w)H = \gamma' H. \tag{1}$$

Normalization by this reference pressure leads to the following dimensionless group, where the normalized form of each variable is denoted by the "$*$" symbol. Note that the dimensionless fluid pressure is a normalized *excess* pore pressure.

- Normalized fluid pressure

$$p^* = \frac{P + \gamma_w(y-H)}{\sigma'_0} \tag{2}$$

- Normalized flux

$$q^* = \frac{q\mu}{D^2\sigma'_0} \tag{3}$$

- Normalized coordinates

$$x^* = \frac{x}{l} \qquad y^* = \frac{y}{H} \tag{4}$$

- Normalized aperture

$$a^* = \frac{a}{l} \tag{5}$$

2.3 Theoretical model

Fluidization refers to situations in which the total stress tensor $\boldsymbol{\sigma}$ in a saturated material and the pressure of the pore fluid P are such that the *effective stress* tensor vanishes or has at least one vanishing eigen value.

Then, following [8], the key part of the theoretical modeling is to determine the spatial distribution of pore pressure within the specimen to identify the locations in which it reaches (or exceeds) the total stress such that:

$$\sigma'^* := \frac{y-H}{H} + p^*(x,y) \geq 0, \tag{6}$$

Assuming Darcy's flow in a rigid porous layer (figure 1), the pressure at any point of the specimen can be obtained as [8]:

$$P + \gamma_w y = \frac{q}{2\pi K} \int_{-a/2}^{a/2} \sum_{j=-\infty}^{\infty} \sum_{i=-\infty}^{\infty} -1^{|j|} \left[ln\left(\sqrt{(x - i\,l - s)^2 + (y - j2H)^2} \right) \right] ds \tag{7}$$

where K is the hydraulic conductivity and q is the influx rate at the injection point.

2.4 Numerical model

A quantitative approach of the problem requires a full coupling where the solid phase can be deformed under the action of the fluid, and fluid flow depends on this deformation. To this aim, a micro-hydromechanical model, combining the discrete element method (DEM) and a pore scale finite volume (PFV) formulation of the viscous flow of an incompressible pore fluid [9, 10] is used. This method accounts the effect of drag forces but lubrication terms are not included.

3 Results and discussion

3.1 Analytical solution for a single injection

Figure 2 shows the typical the pressure field after Eq. 7 for an aperture of a^*=0.1 (Eq. 5). Near the injection area, the pressure contours tend to concentric half-circular shapes due to the quasi-radial flow distribution. On the other hand, the isolines are horizontal near the side walls, consistently with the no-flux condition (figure 1).

Following section 2.3, the fluidized zone can be identified with respect to the sign of the effective stress when the injected flux is increasing. Therein the extent of the fluidized zone can be defined through the shape of the null-pressure isoline plotted in figure 3. The different regimes described in [5] can be distinguished from this series of plots. Low flux values correspond to the expansion regime in which no fluidization zone is detected (figure 3*a*). As the flux increases, pore pressure keeps building up until it balances the total stress. At this point a fluidized zone starts developing above the injection area, corresponding to the cavity regime (figure 3*b*). Eventually, the fluidized zone reaches the top of the specimen, leading to a chimney of fluidized grains (figure 3*c*). The solution with a wider

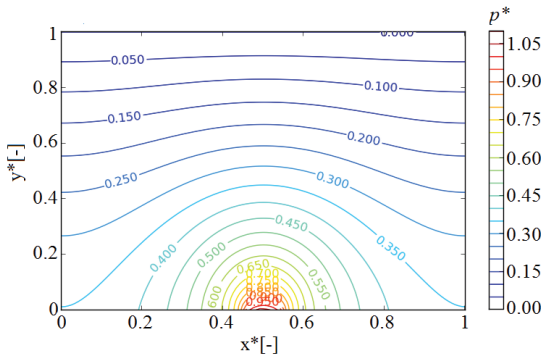

Figure 2. Dimensionless pressure field for an injection rate of q^* = 0.00067 and aperture of a^* = 0.1.

injection area (not shown in the present work) evidences that a slightly larger flow rate is required to initiate the fluidization above a wide aperture. Besides, distinguishing the cavity and the chimney regime in this situation is made uneasy by the fact that large aperture tends to fluidize the granular layer simultaneously at every point in space.

3.2 Numerical simulations for a single injection

Figure 4 shows the evolution of porosity within the granular layer when the injected flux is increasing. The large porosity values at the top of the layer are artifacts and should be disregarded: the particles of the free surface have large porosity values by definition as their Voronoi cells enclose some void space above the free surface. Figure 4 highlights the heterogeneous changes of porosity as localized fluidization starts developing: a cavity appears for q^*=1.16 $\times$ 10^{-3} , followed by a chimney for q^*≥1.45 $\times$ 10^{-3} . In both cases the particles located in the regions of low porosity are moving and have only transient contacts with each other, while the particles of the dense regions are static and contribute to a permanent contact network.

A "bubble" of high porosity is shown in figure 4*c*. Actually this bubble is not fixed in time and space (the figure is only a snapshot at a given time) but tends to move up until it reaches the free surface. Then, another bubble appears at the bottom and move up in a cyclic manner. This is in clear contrast with the cavity regime in plot (*b*) in which the porosity field is stationary.

After setting the injection rate back to zero and reaching a final equilibrium state, an irreversible increment of porosity (n≈ 0.42 locally) is observed above the injection point and throughout the layer (figure 4*d*).

3.3 Aperture size dependency

As mentioned before (see figure 3) and confirmed in figure 5, large apertures (a^* close to 1) lead to the entire liquefaction of the granular assembly rather than forming a cavity and a chimney of fluidization (cavity regime gets narrower near a^* = 1.). The aperture dependency is summarized in the diagram of figure 5 where the different fluidization

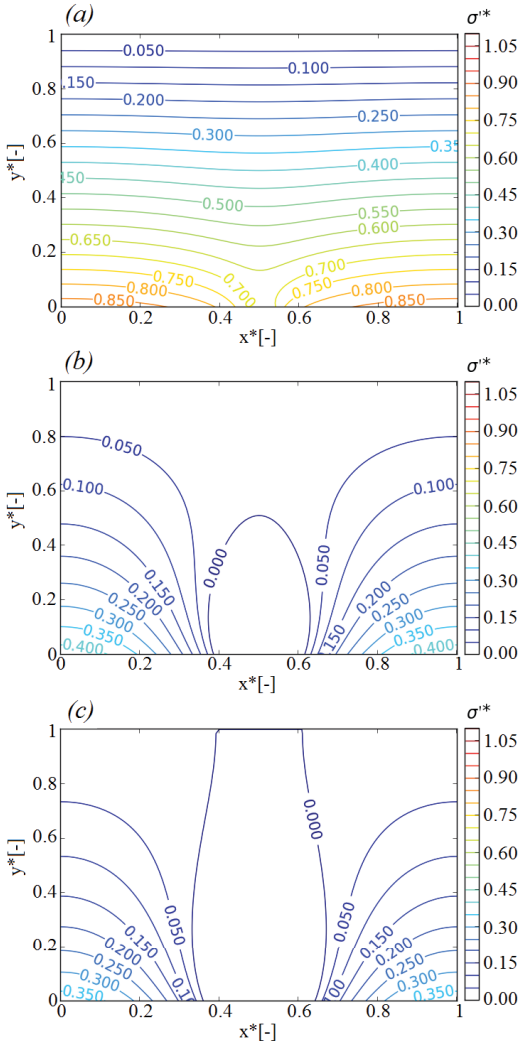

Figure 3. Evolution of the dimensionless effective stress σ^* field when the injected flux increases. Injection aperture a^*=0.1.The normalized fluxes are q^* = 0.00019 (*a*), q^* = 0.00105 (*b*), q^* = 0.00114 (*c*).

regimes are identified from the numerical approach for different combinations of flow rate and aperture

3.4 Two injection points case

Fluidized cavities developing above the injection points are strongly disturbed when two orifices of injection are close to each other. Based on the analytical approach, figure 6 evidences effective stress field at the time when the cavities resulting from two punctual sources are about two merge forming a single chimney. On the contrary, chimneys have individual behavior if the two injection points are sufficiently far from each other.

Figure 7 shows the threshold separating the two behaviors that have been described. Small distances between the injection points lead to a single chimney generated by the two cavities (left part of the diagram in figure 7). On the contrary, cavities are not affected or attracted to each other when the distance between the orifices increases (right part of the diagram in figure 7).

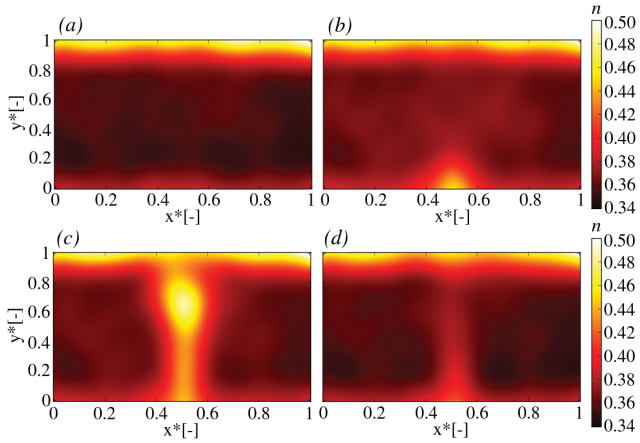

Figure 4. Evolution of the porosity for narrow aperture ($a^* = 0.1$). (*a*) Static regime, $q^* = 0$. (*b*) Cavity regime, $q^* = 0.00116$. (*c*) Chimney regime, $q^* = 0.00145$. (*d*) $q^* = 0$.

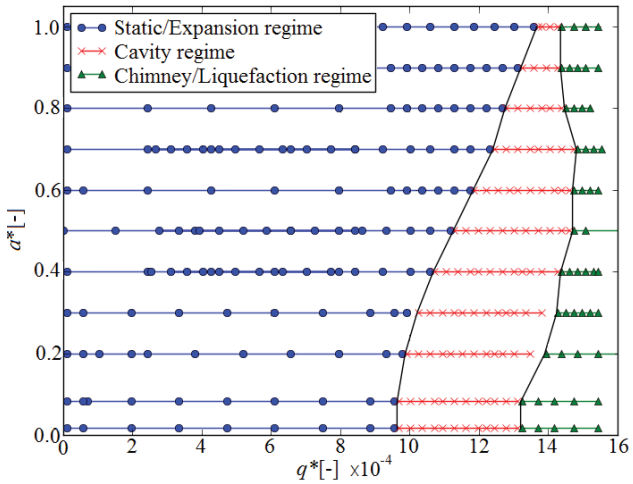

Figure 5. Occurence of the different fluidization regimes (static/expansion, cavity or chimney) depending on aperture a^*. (Determined from the numerical coupled simulations).

4 Conclusions

Both analytical and numerical approaches were presented to characterize the localized fluidization of a granular layer. They are qualitatively in good agreement, with respect to the description of the different fluidization regimes. However, these approaches deviate for large fluxes when a homogeneous permeability field can no longer be assumed. From these approaches, dependency of the fluidization regimes (mainly cavity and chimney) on injection aperture (for a single aperture) and on distance between injection point (for a set of two injections) is given by tracking the vanishing of the effective stress within the granular layer.

References

[1] Payne, Fred C and Quinnan, Joseph A and Potter, Scott T, *Remediation hydraulics* (CRC Press, 2008)

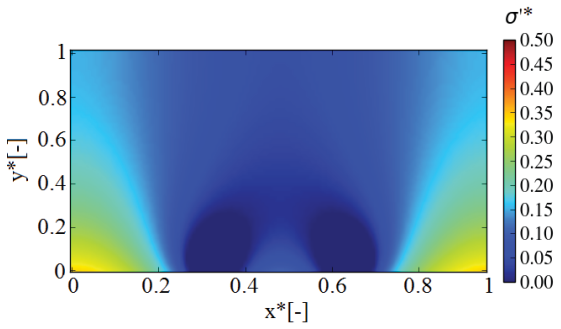

Figure 6. Dimensionless effective stress field for an injection rate of $q^* = 0.00057$ and two punctual sources spaced $\frac{1}{6}$.

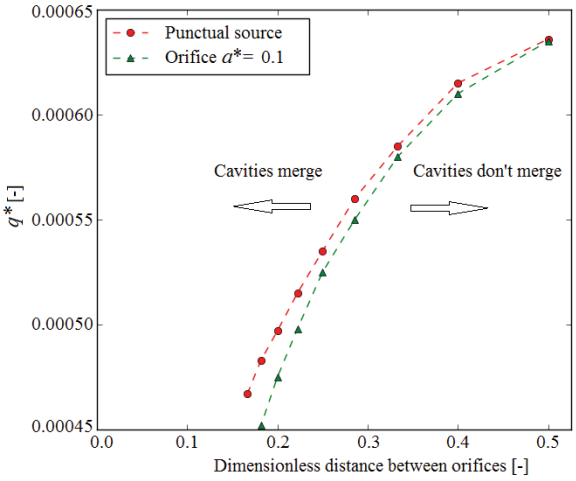

Figure 7. Occurence of cavities merging for two punctual sources and two sources with an aperture of $a^* = 0.1$.

[2] Peng, Yimin and Fan, LT, Chemical Engineering Science, **52**, 2277–2290, (1997)
[3] Weisman, Richard N and Lennon, Gerard P, Journal of waterway, port, coastal, and ocean engineering **120**, 468–487, (1994)
[4] Ngoma, J and Philippe, P and Bonelli, S and Delenne, JY and Radjai, F, Geomechanics from Micro to Macro: Proc. of the Int. Symposium on Geomechanics from Micro to Macro, **4**, 1571–1576, (2014)
[5] P. Philippe and M. Badiane, Physical Review E **87**, 042206, (2013)
[6] Zoueshtiagh, Farzam and Merlen, Alain, Physical Review E **75**, 056313, (2007)
[7] Xilin Cui, Jun Li, Andrew Chan, and David Chapman, Powder Technology **254**, 299-306, (2014)
[8] E. P. Montellà, M. Toraldo, B. Chareyre and L. Sibille, Physical Review E, **94**, 052905, (2016)
[9] Catalano, E and Chareyre, B and Barthélemy, E, International Journal for Numerical and Analytical Methods in Geomechanics **38**, 51–71, (2014)
[10] Chareyre, B and Cortis, A and Catalano, E and Barthélemy, E, Transport in porous media **94**, 595–615, (2012)